Understanding the Electronic Energy Transfer Pathways in the Trimeric and Hexameric Aggregation State of Cyanobacteria Phycocyanin within the Framework of Förster Theory

Yanliang Ren,[†[a]] Bo Chi,[†[a]] Osama Melhem,[[a]] Ke Wei,[[a]] Lingling Feng,[[a]] Yongjian Li,[[a]] Xinya Han,[[a]] Ding Li,[[a]] Ying Zhang,[[a]] Jian Wan,*[[a]] Xin Xu,*[[b]] and Minghui Yang[[c]]

In the present study, the electronic energy transfer pathways in trimeric and hexameric aggregation state of cyanobacteria C-phycocyanin (C-PC) were investigated in term of the Förster theory. The corresponding excited states and transition dipole moments of phycocyanobilins (PCBs) located into C-PC were examined by model chemistry in gas phase at time-dependent density functional theory (TDDFT), configuration interaction-singles (CIS), and Zerner's intermediate neglect of differential overlap (ZINDO) levels, respectively. Then, the long-range pigment-protein interactions were approximately taken into account by using polarizable continuum model (PCM) at TDDFT level to estimate the influence of protein environment on the preceding calculated physical quantities. The influence of the short-range interaction caused by aspartate residue nearby PCBs was examined as well. Only when the protonation of PCBs and its long- and short-range interactions were properly taken into account, the calculated energy transfer rates ($1/K$) in the framework of Förster model at TDDFT/B3LYP/6-31+G* level were in good agreement with the experimental results of C-PC monomer and trimer. Furthermore, the present calculated results suggested that the energy transfer pathway in C-PC monomer is predominant from β-155 to β-84 ($1/K = 13.4$ ps), however, from α-84 of one monomer to β-84 ($1/K = 0.3$–0.4 ps) in a neighbor monomer in C-PC trimer. In C-PC hexamer, an additional energy flow was predicted to be from β-155 (or α-84) in top trimer to adjacent β-155 (or α-84) ($1/K = 0.5$–2.7 ps) in bottom trimer.

DOI: 10.1002/jcc.23221

Introduction

Photosynthesis in green plants, algae, and many species of bacteria is one of the most important biochemical processes on earth. The light energy is absorbed by the antenna light-harvesting system, and then the excitation energy can be very effectively transferred to the photosynthetic reaction center of Photosystem II.[1] The major light-harvesting components in cyanobacteria and red algae are phycobiliproteins, such as phycorerythrin (PE), phycocyanin (PC), and allophycocyanin (APC). These phycobiliproteins assemble into large structures known as phycobilisomes. In phycobilisomes, the light energy is transferred from PE through PC to APC, the entirely procedure typically occurs in 100–200 ps with 90% or higher efficiency over an array of several hundred chromophores.[2] The role of these phycobiliproteins have been studied extensively,[3] but the electronic energy transfer (EET) pathways within phycobiliproteins have not be elucidated in detail yet.

C-phycocyanin (C-PC) belongs to one of the principal components of phycobiliproteins in cyanobacteria. It was found as a complex solution of trimers ($\alpha_3\beta_3$), hexamers ($\alpha_6\beta_6$), and other oligomers, where each α polypeptide subunit has one chromophore known as phycocyanobilin (PCB, a derivative of an open-chain tetrapyrrole) and each β subunit has two PCBs.[4] The sequence of the amino acids for C-PC is clear, where PCBs are located at α-84, β-84, and β-155, respectively.[5–8] After absorption of light energies, the excitation energy on each PCB can be efficiently transferred to neighbor PCB up to distances of several tens of angstroms by the process of EET.[9]

[a] *Y. Ren, B. Chi, O. Melhem, K. Wei, L. Feng, Y. Li, X. Han, D. Li, Y. Zhang, J. Wan*
Key Laboratory of Pesticide and Chemical Biology (CCNU), Ministry of Education, Department of Chemistry, Central China Normal University, Wuhan 430079, People's Republic of China

[b] *X. Xu*
Shanghai Key Laboratory of Molecular Catalysis and Innovative Materials, Ministry of Education (MOE) Laboratory for Computational Physical Science, Department of Chemistry, Fudan University, Shanghai 200433, People's Republic of China

[c] *M. Yang*
Wuhan Institute of Physics and Mathematics, Chinese Academy of Sciences, Wuhan 430071, People's Republic of China
Fax: +86-27-67862022.
E-mail: jianwan@mail.ccnu.edu.cn or xxchem@fudan.edu.cn
[†]These authors contributed equally to this work.

Contract/grant sponsor: National Basic Research Program of China (973 Program); Contract/grant numbers: No. 2010CB126100; Contract/grant sponsor: Natural Science Foundation of China; Contract/grant numbers: 21202056, 21172089, 21072073, and 30900054; Contract/grant sponsor: PCSIRT; Contract/grant number: IRT0953; Contract/grant sponsor: Natural Science Foundation of Hubei Province; Contract/grant number: 2010CDB01202; Contract/grant sponsor: Program for Academic Leader in Wuhan Municipality; Contract/grant number: 201150530150; Contract/grant sponsor: CCNU from the Colleges' Basic Research and Operation of MOE; Contract/grant number: CCNU10C01002 and CCNU10A02006.

There are two kinds of approximated models[4] which can depict the mechanisms of EET between chromophores. In the strong coupling limit, exciton coupling may occur such that a pair of pigments behave as if they were one unit, sharing delocalized energy.[4,10,11] Conversely, in the weak coupling limit, the energy can be localized on each chromophore at a time such that the individual chromophores tend to retain their spectra, respectively.[4] Previously, we have studied the absorption and CD spectra of the C-PC monomer, including both of α and β subunits, by using time-dependent density functional theory (TDDFT),[12,13] strongly supporting that the weak coupling might be the predominant mechanism in the EET among the PCBs in C-PC.

For the case of weak coupling of EET, Förster theory[14] have been generated half century ago and used to satisfactorily depict the weak coupling mechanism of EET. Sauer and coworkers[15,16] have systematically investigated rate constants (K) for energy transfer in the monomeric and trimeric C-PC from cyanobacterium *Synechococcus sp. PCC7002* using the following Förster equation of resonant energy transfer in the weak coupling limit:

$$K = \mathrm{C} \cdot G \cdot \mathrm{S} \cdot \mathrm{I} \tag{1}$$

where C is a collection of constants, G ($G = \frac{\kappa^2}{R_{DA}^6}$,$\kappa$, the orientation factor) is a geometric term dependent on the relative orientation and distance between the donor and acceptor chromophores, S is a collection of spectroscopic properties of the individual chromophores, and I is the integral of the overlap of the fluorescence spectrum of the donor with the absorbance spectrum of the acceptor. In addition to the relative distances and orientations between chromophores, obtained from the crystal structure of C-PC, the calculations of rate constant by eq. (1), therefore, require spectroscopic resolution of several properties of the chromophores (α-84, β-84, and β-155) found in C-PC monomeric and trimeric aggregation state, including absorption and fluorescence spectra, molar absorptivities, fluorescence quantum yields, and fluorescence lifetimes.

On the other hand, the Förster formula for predicting EET rate constant (K) of the weak coupling model from a donor (D) to an acceptor (A) can also be extended to the following equation according to the Fermi golden rule[9,17]:

$$K = \frac{1}{\hbar^2 c}|V_{DA}|^2 J \tag{2}$$

where V_{DA} represents the contribution from the electronic couplings of excited states between D and A. J denotes the spectral overlap factor.[9] Under the dipole–dipole approximation, V_{DA} can be further expressed as the following equation[17]:

$$V_{DA}^{d-d} = \frac{1}{4\pi\varepsilon_0}\kappa\frac{|\mu_D||\mu_A|}{n^2 R^3} \tag{3}$$

where $|\mu_D|$ and $|\mu_A|$ are the magnitude of transition dipole moments for the donor and acceptor chromophores in Debye (D). n is the refractive index of the surrounding medium (unitless).[18] The $1/n^2$ also can be regarded as the screening factor s.[19,20] R is the mass-center-to-mass-center separations between D and A. κ denotes the orientation factor,[17] the same parameter as that in eq. (1), $\kappa \equiv \hat{\mu}_D \cdot \hat{\mu}_A - 3(\hat{\mu}_D \cdot \hat{r}_{DA})(\hat{\mu}_A \cdot \hat{r}_{DA})$, where $\hat{r}_{DA}$ is the unit vector along the line connecting the mass centers of the two chromophores; $\hat{u}_D$ and $\hat{u}_A$ are unit vectors in the directions of the transition dipole moments for the donor and acceptor chromophores (unitless). Similarly, the orientation factor (κ) can also be written as following: $\kappa \equiv \cos\gamma - 3\cos\alpha\cos\beta$, where α and β are the angles between $\hat{u}_D/\hat{u}_A$ and $\hat{r}_{DA}$; γ is the angle between $\hat{u}_D$ and $\hat{u}_A$, as illustrated in Figure 1.

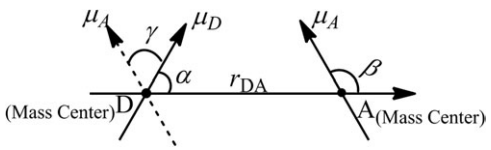

Figure 1. The angles α, β, and γ defining the relative orientation of the electronic transition dipole moments in donor (D) and acceptor (A) in orientation factor (κ) calculations.

A central important ingredient of eq. (2) is the electronic coupling (V), a key parameter in EET calculation, which usually controls the magnitude of the energy transfer.[21–26] In the past decade, much theoretical attempts have been addressed the accurate prediction of electronic couplings from quantum mechanical methods,[27–32] Especially, using dipole–dipole approximation [eq. (3)] and transition density cube (TDC) model,[33] Scholes et al. have successfully calculated the electronic coupling of the phycoerythrin 545 from *cryptophyte algae* at CIS/6-31G level. Their results suggested that when the separations between chromophores were larger than 20 Å, the dipole–dipole approximation was adequate for describing the electronic coupling between chromophores.[18,33,34]

To theoretically calculate the energy transfer rates within the Förster model, the spectral overlap (J) is another important term need to be estimated under certain approximation. A pioneer work about the spectral overlap (J) calculations was reported by Scholes et al.[35] By using this calculation method of spectral overlap, they also investigated the EET rates from B800 to B850 (separated by ~9 Å) in light harvesting complex LH2 from *Rps. Acidophila* at CIS/6-31G* level, in which the electronic couplings (V) were studied by TDC model. According to the derivations of Scholes et al., the spectra overlap part of eq. (2) can be expressed as following:[35] $J = \int_0^\infty f_A^{Norm}(\nu) f_D^{Norm}(\nu) d\nu$, where $f_A^{Norm}(\nu)$ and $f_D^{Norm}(\nu)$ are represented the area-normalized absorption and fluorescence line shapes, respectively. To obtain the area-normalized line shapes, $f_A^{Norm}(\nu) = N_A f_A(\nu)$, $f_D^{Norm}(\nu) = N_D f_D(\nu)$, therefore, the spectra overlap term can be written as following:

$$J = \int_0^\infty N_A f_A(\nu) N_D f_D(\nu) d\nu \tag{4}$$

where N_A and N_D are normalization factor, respectively, such that $1/N_A = J = \int_0^\infty d\nu f_A(\nu)$ and $1/N_D = J = \int_0^\infty d\nu f_D(\nu)$, whereas $f_A(\nu)$ and $f_D(\nu)$ are the line shapes of acceptor absorption spectrum and donor emission spectrum, ν is in wavenumber (cm^{-1}).

The EET rate between chromophores can be directly calculated at one theoretical level in term of the eqs. (2)–(4), which, therefore, provides us a useful theoretical tool to understand and predict the EET pathways within biosystems like phycobiliproteins. In the

present study, the corresponding excited states and transition dipole moments of PCBs located into C-PC were examined by model chemistry in gas phase at TDDFT, CIS, and ZINDO levels, respectively. Then, the long-range pigment-protein interactions were approximately taken into account by using polarizable continuum model (PCM) at TDDFT level to estimate the influence of protein environment on the preceding calculated physical quantities. The influence of the short-range interaction caused by aspartate residue nearby PCBs was examined as well. When the protonation of PCBs and its short- and long-range interactions with the protein moiety were properly taken into account, the energy transfer rates (1/*K*) were calculated in the framework of Förster model at TDDFT level. The influences of orientation factors, magnitude of transition dipole moments, and spectral overlaps on the EET rates were discussed in detail, respectively, based on the present calculated results.

The present article is organized as follows. In Computational details section, we outline the computational details. Calculation results and discussions are presented in Results and discussion section. A summary is given in Conclusion section.

Computational Details

The electronic coupling in the present study was calculated in term of eq. (3), in which $n^2 = 2$ is used for proteins environment.[36] Then, the initial geometries were set up according to the data set of crystal structures of C-PC isolated from *S. platensis*[37] (PDB ID:1HA7, resolution of 2.2 Å), the hydrogen atoms were added by using Gaussview 3.07. Although the crystal structures are unable to show an evidence for protonation, our previous calculations[12,13] demonstrated that protonation was most likely exist in PCBs. To examine the influences of protonations and short-range interactions caused by aspartate residue nearby PCBs on the electronic coupling, the present calculations, therefore, were performed at three levels of model chemistry from simple to more sophisticated model systems in gas phase. Model I was a neutral PCB molecule, a protonated PCB molecule ($PCBH^+$) was taken as Model II. Model III (as shown in Fig. 2) consisted of a $PCBH^+$ molecule and an aspartate residue. The geometry optimizations of three models were also carried out by using B3LYP flavor[38–40] of DFT, with 6-31G* basis set[41] in *vacuo*. To calculate excited state associated physical quantities, the molecular geometry usually need to be optimized first within the framework of vertical excitations. However, the centers–of-mass of optimized PCBs may change (orientation and geometrical parameters) compared with the centers-of-mass of PCBs initial geometries in crystal structures. Therefore, in the current optimization procedure of Gaussian 03, the keyword "no symmetry" was used to prevent the reorientation and cause all computations to be performed in the initial input orientation. By using the optimized geometries in *vacuo* of three models, the separations (R and $\hat{r}_{DA}$) between the mass centers of the two PCBs were calculated. Moreover, based upon the optimized geometries, the excited states of PCBs with three models were performed at TDDFT-B3LYP/6-31+G* level as well, and the excited states with lowest excitation energies were used, to obtain the excitation energies and transition dipole moments for the next EET calculations.

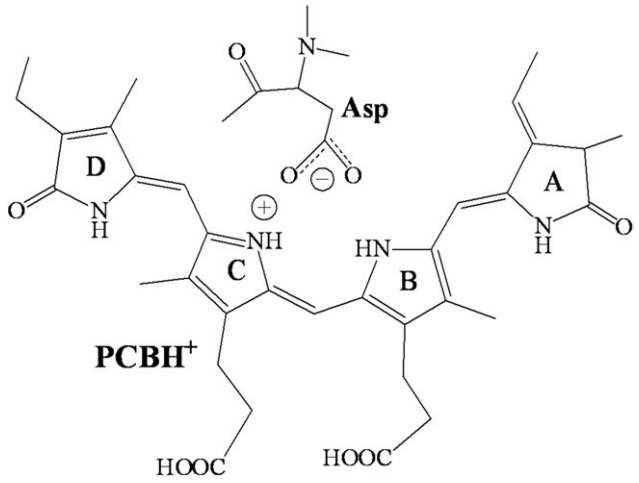

Figure 2. Model III consisting of $PCBH^+$ and the aspartate residue for PCBs, where —COOH and NH_2 are replaced by —$COCH_3$ and —$N(CH_3)_2$.

Based upon the model III in gas phase [Model III (GAS)], additional calculations were further performed to decompose the influencing effects: (1) the excited states calculations were performed at TDDFT-B3LYP 6-31G, 6-31+G*, and 6-311+G* levels to check the basis sets dependence. (2) The excited states calculations were also carried out at TDDFT-PBEH1PBE/6-31+G(d), CIS/6-31+G(d), and ZINDO levels to examine the differences of the excitation energies and transition dipole moments calculations with various theoretical methods.

To examine the influence of protein environment on the excitation energies and transition dipole moments, the long-range pigments-protein interactions were approximately taken into account by using PCM at TDDFT-B3LYP level with Model III [Model III (PCM)], in which the typical value used is $\varepsilon = 4.0$,[42–44] ε (infinity) $= 1.776$. The details and reliabilities of these calculations for low-lying excited states have been well-documented in our previous studies.[12,13]

The spectra overlaps (J) were calculated in term of eq. (4) mentioned-above, the spectral overlap between A and D is quite dependent on the line shapes of the acceptor and donor spectra. Thus, based upon the excitation energies of individual PCBs, the absorption spectra of acceptors were approximately fitted by Gaussian function (with a full width at half-maximum of 400 cm^{-1})[45] to obtain the line shapes of corresponding PCBs. The reliability of fitting absorption spectra line shapes for PCBs of C-PC in monomer have been well documented in our previous studies.[12,13] To obtain the donor emission line shapes of the PCBs, we mirror the corresponding absorption spectrum and plus red-shift around 550 cm^{-1} (corresponding to 20 nm, Stokes shift of PCBs[7]), which has been proposed in the previous study.[17] Then, both the absorption and emission line shapes were carefully normalized to unit area in wavenumber (cm^{-1}) scale in term of eq. (4), without taking vibrational effects into account. Considering the importance of protonation of PCBs and the role played by aspartate residue, the energy transfer rates constants (K) calculations were further used by adopting the Model III (PCM).

All of the geometry optimization, excitation energies and transition dipole moment mentioned-above were performed by using the Gaussian 03 suite of program.[46]

Results and Discussion

The effects of the optimized geometries on the separations and orientations

To estimate the effects of the optimized geometries on the separations and orientations of donor–acceptor pairs, the center of mass between PCBs initial geometries adopted from crystal data and the optimized PCBs geometries in Model III were compared with each other, and summarized in Supporting Information Table S5, the superposition pictures of the initial PCBs and the optimized PCBs were also illustrated in Supporting Information Figure S1. Compared with the initial PCBs, the center-of-mass of optimized PCBs were changed about 0.01–0.07 Å. Compared with the separations of the initial D–A pairs (i.e., crystal structural data), the separations of the optimized D–A pairs changed about 0.01–0.12 Å. Figure S1 in Supporting Information illustrated that the orientation of the optimized PCBs was kept in the initial PCBs orientation, the corresponding root-mean-squared deviation (RMSD) values of atom coordinates between optimized and initial PCBs were 0.42–1.56 Å. These comparison results suggested that the influence of the present optimizations on the separations and orientation of donor–acceptor pairs were actually small, considering the crystallographic resolution of 2.2 Å.

In addition, the same chromophores in different subunits (e.g., α^1-84 and α^2-84, or β^1-84 and β^3-84) have different geometric parameters (bond lengths, angles, dihedrals, etc.). These differences mainly originated from two parts in the present study. First, due to the crystallographic resolution limitation (2.2 Å), subunits located into C-PC trimer and hexamer may have tiny geometry differences, including PCBs chromophores. We have examined, α^1-84 and α^2-84 as an example, their geometrical differences using crystal structure data directly. The RMSD value of atom coordinates between α^1-84 and α^2-84 initial geometries adopted from crystal structure is 0.3 Å (Figure S2A in Supporting information). Second, with different initial geometries, the optimization calculations may get more different finally optimized geometries. For example, the RMSD value of atom coordinates between α^1-84 and α^2-84 optimized geometries is increasing to 0.9 Å (Figure S2B in Supporting information). We do not think these small geometry differences reflect the environmental effects from the protein subunits, just attribute them to the crystallographic resolution limitation and subsequent optimizations.

The electronic coupling

The electronic couplings are dependent upon the separations, orientation factors, and transition dipole moments of donor–acceptor pair in term of eq. (3). To examine the effects of theoretical methods on the excitation energies and transition dipole moments, the calculations with model III were carried out in gas phase by using TDDFT-B3LYP, TDDFT-PBEH1PBE, CIS, and ZINDO methods, respectively, as listed in Table S1 of Supporting Information. The corresponding orientation factors (κ) and electronic couplings ($|V|^2$) for different theoretical methods were summarized in Table S2 of Supporting Information. As listed in Supporting Information Tables S1 and S2, the CIS calculations remarkably overestimated the excitation energies (~430 nm), comparing with the experimental values (594–624 nm). The deficiency of CIS methods mainly own to the neglect of σ-π dynamic correlation, as suggested in precede study.[27] ZINDO calculations in gas phase predicted lower excitation energies (–630 nm), looked better and close to the experimental values (594–624 nm). However, our further test calculations indicated that the solvent effect on the excitation energy at ZINDO level was about 130 nm red-shift, which led to a significant deviation of ZINDO excitation energies compared to the experimental values. Conversely, both TDDFT-B3LYP and TDDFT-PBEH1PBE predicted similar excitation energies (550–560 nm) and transition dipole moments (11.8–12.3 D), the excitation energies of TDDFT-B3LYP are slightly lower than those of TDDFT-PBEH1PBE. The absolute values of orientation factor (κ) calculated by these four methods were very close to each other, whereas the calculated transition dipole moments were changed within 1.5–3.0 D deviation.

Additionally, the influences of basis sets on the excitation energies, transition dipole moments were estimated and collected in Table S3 of Supporting Information. The corresponding electronic couplings ($|V|^2$) and orientation factor (κ) calculated by three different basis sets were summarized in Table S4 of Supporting Information. Our calculations showed that both 6-31+G* and 6-311+G* basis sets gave the similar excitation energies (560–566 nm), in contrast, 6-31G basis sets overestimated the excitation energies (~550 nm). Correspondingly, transition dipole moments of PCBs computed by 6-31G basis sets were subtly larger compared to those of both 6-31+G* and 6-311+G*, which, in turn, resulted in the greater values of electronic coupling ($|V|^2$). 6-31+G* basis sets gave the similar excitation energies, transition dipole moments, and electronic coupling with those obtained by 6-311+G* basis sets. Considering the balance between computational cost and calculation accuracy, TDDFT/B3LYP/6-31+G* level was adopted finally for the next EET rates calculations.

The transition dipole moments of PCBs in C-PC trimer under three models (Models I–III) were calculated at TDDFT-B3LYP/6-31+G* level, as summarized in Table 1. The corresponding separations (R), orientation factors (κ), and electronic couplings (V) were summarized in Table 2. The β^1-155→α^1-84, β^1-155→β^1-84, and α^1-84→β^1-84 represent the possible energy transfer pathways in C-PC monomer, whereas the α^2-84→β^1-84, α^1-84→β-84, and β^1-155→α^2-84 indicate the possible energy transfer pathways from one monomer to adjacent monomer in C-PC trimer, respectively. As listed in Table 2, the electronic coupling $|V|^2$ values calculated with protonation (Model II) were approximately two-times larger than those without protonation (Model I). In addition, one can see from Table 1 that the magnitude of transition dipole moments of PCBs in Model II increased about 1.6 D. However, small changes were observed in Table 2 for the calculations of the

Table 1. The transition dipole moments of PCBs in C-PC trimer calculated at TDDFT-B3LYP/6–31+G* level within various models.

	Transition dipole moments (D[a])				
Models	α^1-84	β^1-84	β^1-155	α^2-84	β^3-84
Model I[b]	11.1	11.1	10.8	11.1	11.2
Model II[c]	12.8	12.9	12.0	12.8	12.9
Model III (GAS)[d]	11.9	11.8	12.0	10.3	11.9
Model III (PCM)[e]	13.4	13.5	13.1	13.2	13.5

[a] Debye. [b] The neutral PCB molecule. [c] The protonated PCB molecule ($PCBH^+$) is calculated in the gas phase. [d] The complex consisted of a $PCBH^+$ molecule and an aspartate residue calculated in the gas phase. [e] The complex environment (protein and water) was modeled using the PCM model.

separations and the orientation factor (κ) in Models I and II. By these analysis, we concluded that the protonation of PCBs mainly lead to increase of the magnitude of transition dipole moments, which, in turn, induced the increase of the electronic coupling $|V|^2$. Our previous studies[12,13] have demonstrated the protonation enhanced the conjugation effect in B and C ring of PCBs. Hence, the increase of the conjugation of PCBs by protonation might be responsible for the increase of magnitude of transition dipole moments.

The short-range interactions[7–9] caused by aspartate residue nearby PCBs were also examined in Model III (GAS). An important finding was that, Model III (GAS) computed the magnitude of transition dipole moments of α^1-84, β^1-84, and β^3-84 at 11.9, 11.8, and 11.9 D, respectively, which were decreased about 1.0–2.5 D as compared to those of Model II (Table 1). Our previously studies[12,13] have disclosed that the carboxylate oxygens in the aspartate residue were actually involved in the hydrogen bonding with the B and C rings in PCBs. These hydrogen bonds, therefore, likely weakened the conjugation effect of four pyrrolic rings, which, in turn, induced the decrease of transition dipole moments magnitude. As expected from eq. (3), the electronic couplings calculated with Model III (GAS) exhibited almost two-fold decrease compared to those with Model II, especially for the α^2-84→β^1-84 and α^1-84→β^3-84 EET pathways (see Table 2 for details).

From Table 1, we observed that the transition dipole moment (10.3 D) of α^2-84 with Model III (GAS) calculated at TDDFT/B3LYP/6-31+G* was obviously smaller than the values of other PCBs (∼11.9 D). However, using additional methods TDDFT-PBEH1PBE and CIS with 6-31+G* basis set, even using the same TDDFT-B3LYP flavor with different basis sets (6-31G and 6-311+G*), the calculated transition dipole moments of α^2-84 with Model III (GAS) were always larger than 11.0 D and with the similar magnitude to those of other PCBs (see Supporting Information Tables S1 and S3 for details). Furthermore, the transition dipole moment value (13.2 D) of α^2-84 with Model III (PCM) calculated at TDDFT-B3LYP/6-31+G* level was "recovered" and almost consistent with those of other PCBs (13.1–13.5 D) at this level. The reason for this exceptional performance of Model III (GAS) at TDDFT/B3LYP/6-31+G* is unclear.

Model III (PCM) includes the short-range interaction from the nearby amino acid and the long-range interaction from the protein pocket. With PCM model, the magnitudes of transition dipole moments were increased by 1.5–2.9 D, which, in turn, resulted in the increase of electronic couplings $|V|^2$ by twice (Table 2). Similar to the protonation effects, solvent effects (PCM) led to the increases of the transition dipole magnitude, while small changes of the separations and orientation factors. Importantly, one can see from Table 1 that the change trend of transition dipole moments magnitude was Model I < Model II > Model III (GAS) < Model III (PCM). Interestingly, the calculated electronic coupling ($|V|^2$) generally followed this change trend (Table 2). It is clear from eq. (3) that the transition dipole moments of D and A chromophores are central important factors in the electronic coupling calculations.

In addition to the transition dipole moments of PCBs, it is clear from Table 2 that the electronic coupling ($|V|^2$) significantly depended on the separation (R) and orientation factor (κ). For example, in Model III (PCM), larger $|V|^2$ value of α^2-84→β^1-84 (or α^1-84→β^3-84) would be attributed to the short R (∼20 Å), because $|V|^2$ values are inversely proportional to R^6 according to the eq. (2). Conversely, in Model III (PCM), the pathway of β^1-155→α^1-84 and α^1-84→β^1-84 have quite different $|V|^2$ values, even if their R values are similar each other (47–50Å). This difference may be attributed to the orientation factor (κ). Since the $|V|^2$ are proportional to κ^2, the κ values of α^1-84→β^1-84 is 18-fold larger than those of β^1-155→α^1-84, this means that the $|V|^2$ values of α^1-84→β-84 should be at least 324-fold larger than those of β^1-155→α^1-84. As listed in Table 2, the $|V|^2$ value of α^1-84→β^1-84 is actually 550-fold larger than those of β^1-155→α^1-84. Correspondingly, the smaller $|V|^2$ value of β^1-155→α^2-84 (1.4 cm^{-2}) may be contributed to the smaller

Table 2. The donor–acceptor separations (R), electronic couplings ($|V|^2$), and orientation factor (κ) between PCBs in C-PC trimer within three models.

	Model I[b]			Model II[c]		Model III (GAS)[d]			Model III (PCM)[e]	
D–A pairs[a]	R (Å)	κ	$\|V\|^2$ (cm^{-2})	κ	$\|V\|^2$ (cm^{-2})	R (Å)	κ	$\|V\|^2$ (cm^{-2})	κ	$\|V\|^2$ (cm^{-2})
β^1-155→α^1-84	48.1	−0.1	0.6	−0.1	0.5	46.9	0.1	0.2	−0.1	0.3
β^1-155→β^1-84	35.3	0.6	62.9	0.7	139.3	33.0	−0.6	120.3	−0.6	189.3
α^1-84→β^1-84	50.2	−1.8	77.4	−1.7	121.5	49.8	−1.8	99.4	1.8	164.8
α^2-84→β^1-84	20.2	−1.5	12422.4	−1.5	22502.0	20.4	1.5	11454.0	1.5	24593.0
α^1-84→β^3-84	20.1	−1.5	12613.6	−1.5	22174.0	20.3	−1.4	14669.0	1.4	23762.2
β^1-155→α^2-84	38.6	0.1	1.0	0.1	1.0	38.8	0.1	0.6	0.1	1.4

[a] Donor–Acceptor pairs. [b] The neutral PCB molecule. [c] The protonated PCB molecule ($PCBH^+$) calculated in the gas phase. [d] The complex consisted of a $PCBH^+$ molecule and an aspartate residue calculated in the gas phase. [e] The protein environment was modeled using the PCM model.

Table 3. The angles α, β, and γ of the electronic transition dipole moments in donor ($\hat{u}_D$) and acceptor ($\hat{u}_A$), and the unit vector ($\hat{r}_{DA}$) between two PCBs with Model III in PCM, together with the corresponding orientation factors (κ).

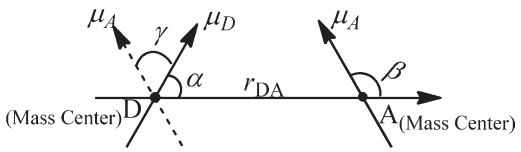

D–A pairs[a]	α (°)	β (°)	γ (°)	κ
β^1-155→α^1-84	77.2	47.4	67.6	−0.1
β^1-155→β^1-84	91.5	75.1	125.1	−0.6
α^1-84→β^1-84	167.9	23.2	161.3	1.7
α^2-84→β^1-84	31.2	143.5	126.0	1.5
α^1-84→β^3-84	146.5	38.0	123.9	1.4
β^1-155→α^2-84	92.5	90.7	85.4	0.1

[a] Donor–Acceptor pairs.

κ value (0.1). These results suggested that the orientation factor was another key factor in the electronic coupling ($|V|^2$) calculations.

To understand the physical picture of orientation factors (κ), with model III (PCM), the angles α, β, γ of the electronic transition dipole moments in donor ($\hat{u}_D$) and acceptor ($\hat{u}_A$), and the unit vector ($\hat{r}_{DA}$) between two chromophores were listed in Table 3. As can be seen from Table 3, when the angles α, β, and γ were closed to 0° and 180°, the energies transfer pathways remarkably exhibited higher orientation factors (κ) (>1.5), such as α^1-84→β^1-84, α^2-84→β^1-84, and α^1-84→β^3-84. In contrary, when the angles α, β, and γ were closed to 90°, the corresponding orientation factors (κ) were much smaller (<0.1), such as β^1-155→α^1-84, β^1-155→β^1-84, and β^1-155→α^2-84. One can conclude that the parallel orientations of $\hat{u}_D$, $\hat{u}_A$, and $\hat{r}_{DA}$ are in favor of the energies transfer, whereas perpendicular orientations of $\hat{u}_D$, $\hat{u}_A$, and $\hat{r}_{DA}$ are not conducive to the energies transfer. Therefore, the κ values of α^1-84→β^1-84 was the largest (in Table 3), mainly owning to angles α and γ were closed to 180°, and the angle β was closed to 0°. The relative orientations of transition dipole moments of PCBs in trimer were also shown in Figure 3.

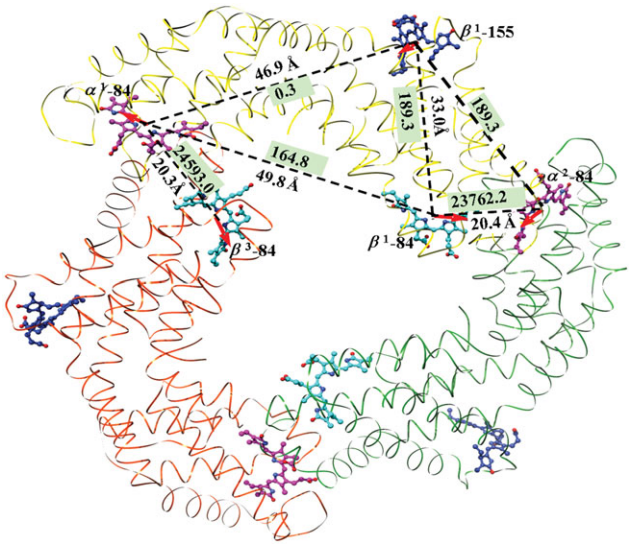

Figure 3. The schematic of separations, electronic couplings ($|V|^2$), and orientations of transition dipole moment of PCBs in C-PC trimer calculated at TDDFT-B3LYP/6-31+G* level with Model III (PCM). The structural models of PCBs are shown in colored stick-ball. The dashed lines indicate the center-to-center separations between the PCBs, red arrows indicate the orientations of electronic transition dipole moments of PCBs.

Table 4. The comparison of experimental and theoretical energy transfer rates (1/K) with Model III (PCM) between PCBs in C-PC monomer, trimer, and hexamer.

D–A pairs[a]	Model III (PCM) $\lvert V\rvert^2$ (cm^{-2})	J (cm)	K (ns^{-1})	1/K (ps)	$1/K_{expt.}$ (ps)[b]
β^1-155→α^1-84	0.3	4.2E−04	0.2	6099.9	>500
β^1-155→β^1-84	189.3	3.3E−04	74.6	13.4	45 ± 15
α^1-84→β^1-84	164.8	8.5E−05	16.5	60.5	200 ± 70
α^2-84→β^1-84	24593.0	8.8E−05	2545.0	0.4	0.1[c]–1.0[b]
α^1-84→β^3-84	23762.2	1.2E−04	3252.6	0.3	/
β^1-155→α^2-84	1.4	4.1E−04	0.7	1497.8	/
β^1-155 →β^4-155	1136.4	1.5E−03	2024.8	0.5	/
β^1-84→β^6-84	202.2	1.4E−04	34.4	29.1	/
α^2-84→α^4-84	2437.4	1.3E−04	368.1	2.7	/

[a] Donor–Acceptor pairs. [b] Ref. [15]. [c] Ref. [47].

Electronic energy transfer pathways

The energy transfer rates between PCBs in C-PC monomer, trimer and hexamer calculated at TDDFT-B3LYP/6-31G* level with Model III (PCM) together with experimental results were list in Table 4, corresponding energy transfer pathways were schematically represented in Figure 4 as well. In C-PC monomer, there were three possible energy transfer pathways, such as β^1-155→β^1-84(13.4 ps), α^1-84→β^1-84 (60.5 ps), and β^1-155→α^1-84(6099.9 ps). For these three pathways, the smallest electronic transfer rate (1/K) was of β^1-155→α^1-84, whereas the largest one was of β^1-155→β^1-84, which was in qualitative agreement with the experimental trend in C-PC monomer:[15] β^1-155→β^1-84 (45 ps) < α^1-84→β^1-84 (200 ps) < β^1-155→α^1-84 (>500 ps), as listed in Table 4. The energy transfer rate of β^1-155→α^1-84 exhibit at least 100-times slower than another two, therefore, the energies flows in monomer are likely transferred via β^1-155→β^1-84 and α^1-84→β^1-84 pathways (Fig. 4).

In the C-PC trimer, we investigated additional two EET pathway rates, β^1-155→α^2-84 (1497.8 ps) and α^2-84→β^1-84 (0.4 ps) [or α^1-84→β^3-84 (0.3 ps), due to its symmetry]. We found that the energy transfer rate of α^2-84→β^1-84 (0.4 ps) [or α^1-84→β^3-84 (0.3 ps)] exhibited dramatically faster (about 10^2–10^5 times) than other pathways in C-PC monomer and trimer. The present calculated energies transfer rates of β^1-155→α^2-84 and α^1-84→β^3-84 were qualitatively consistent with the previous studies reported by Sauer and coworkers[16] and both of which were in good agreement with the experimental data (0.1–1.0 ps). The qualitative agreements between theoretical and experimental studies suggested that method, density functional, and basis set (TDDFT/B3LYP/6-31+G*) used herein were sufficient to depict the EET pathways in the case of C-PC.

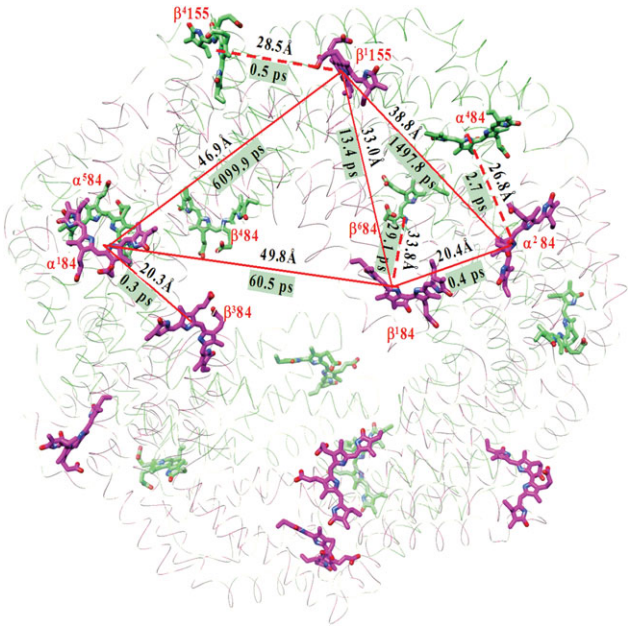

Figure 4. The schematic of separations and theoretical energy transfer rates between PCBs in C-PC hexamer calculated at TDDFT-B3LYP/6-31+G* level with Model III (PCM). The structural models of PCBs are shown in color stick; the pink sticks represent PCBs in top trimer, green sticks represent the PCBs in bottom trimer. The red solid lines indicate the center-to-center separations between the PCBs within top trimer, whereas dashed ones indicate the PCBs separations between top trimer and bottom trimer.

Combining the calculated EET rates in C-PC monomer and trimer mentioned-above, one can conclude that the energy transfer pathway in C-PC monomer is predominant from β^1-155 to β^1-84 (13.4 ps), however, from α-84 of one monomer to β-84 (0.3–0.4 ps) in a neighbor monomer in C-PC trimer.

In previous study, Mimuro et Al.[7,8] proposed the electronic transfer rates only in term of the separations between two chromophores. According to the relative separations of β^1-155→β^1-84 (33.0 Å), β^1-155→α^2-84 (38.8 Å), and α^2-84→β^1-84 (20.4 Å), they supposed that additional possible energy transfer pathway is from β^1-155 to β^1-84 in same monomer via the α^2-84 in adjacent monomer. However, our calculations showed that this pathway was unfeasible. The present calculated transfer rate between β^1-155 and α^2-84 (in adjacent monomer) was 1497.8 ps, which was dramatically smaller than the rate (13.4 ps) between β^1-155 and β^1-84 in same monomer. Our electronic transition dipole moments orientations analysis in Table 3 showed that, for β^1-155→α^2-84, the nearly perpendicular orientations of $\hat{u}_D$, $\hat{u}_A$, and $\hat{r}_{DA}$(92.5°, 90.7°, 85.4°), led to the smaller orientation factor (0.1), which in turn led to the larger energy transfer rate, although the separation of β^1-155→α^2-84 (~38.6Å) was slightly longer than those of β^1-155→β^1-84 (33.0 Å), as listed in Table 2.

To our knowledge, no experimental or theoretical energy transfer rates in C-PC hexamer were reported. Herein, we have investigated the possible energy transfer pathways in C-PC hexamer within Förster model of eqs. (2)–(4) at TDDFT/B3LYP/6-31+G* level. Our calculation results (Table 4 and Fig. 4) indicated that the favorable energy transfer pathways between two trimers were β^1-155→β^4-155 (0.5 ps) or α^4-84→α^2-84 (2.7 ps), because both EET rates exhibited 10–50 times faster than that of β^1-84→β^4-84 (29.1 ps). Therefore, the predominant EET pathways in C-PC hexamer were likely from β-155 (or α-84) in top trimer to β-155 (or α-84) in adjacent bottom trimer, rather than from β-84 in top trimer to β-84 in adjacent bottom trimer.

Conclusion

We present herein a series of first principles calculations at the various levels of model chemistry to insight the EET pathways in C-PC monomer, trimer and hexamer within the framework of Förster theory. Our results showed that both the short- and long-range interactions between chromophores and environmental protein moiety could influence the magnitudes of transition dipole moments, and consequently affect electronic coupling. Only when the protonation of PCBs and its long- and short-range interactions were properly taken into account, the calculated energy transfer rates (1/*K*) in the framework of Förster model at TDDFT/B3LYP/6-31+G* level were in qualitative agreement with the experimental results of C-PC monomer and trimer. Furthermore, the present calculated energy transfer rates suggested that the predominant EET pathway in C-PC monomer was from β-155 to β-84, whereas the additionally possible predominant EET pathway in C-PC trimer was from α-84 of one monomer to β-84 in a neighbor monomer. Albeit no experimental energy transfer rates between C-PC hexamer was reported, our present theoretically calculated results predicted that the energy flow in C-PC hexamer was most likely transferred from α-84(β-155) in top trimer to adjacent α-84 (β-155) in bottom trimer (1/K = 0.5~2.7 ps). The preceding calculations and discussions showed that the extended Förster model used herein was applicable for us to insight the EET pathways within phycobiliproteins in detail in the near future.

Keywords: electronic energy transfer rates · C-phycocyanin · Förster theory · time-dependent density functional theory

How to cite this article: Y. Ren, B. Chi, O. Melhem, K. Wei, L. Feng, Y. Li, X. Han, D. Li, Y. Zhang, J. Wan, X. Xu, M. Yang, *J. Comput. Chem.* **2013,** *34,* 1005–1012. DOI: 10.1002/jcc.23221

Additional Supporting Information may be found in the online version of this article.

[1] A. N. Glazer, *Annu. Rev. Biophys. Biophys. Chem.* **1985**, *14,* 47.
[2] J. M. Zhang, J. Q. Zhao, L. J. Jiang, X. G. Zheng, F. L. Zhao, H. Z. Wang, *Biochim. Biophys. Acta* **1997**, *1320,* 285.
[3] R. MacColl, D. Guard-Friar, Phycobiliproteins, CRC Press: Boca Raton, FL, **1987**.
[4] R. MacColl, *J. Struct. Biol.* **1998**, *124,* 311.
[5] R. E. Dale, F. W. J. Teale, *Photochem. Photobiol.* **1970**, *12,* 99.
[6] F. W. J. Teale, R. E. Dale, *Biochem. J.* **1970**, *116,* 161.
[7] M. Mimuro, P. Fuglistaller, R. Rumbeli, H. Zuber, *Biochim. Biophys. Acta* **1986**, *848,* 155.
[8] M. Mimuro, R. Rümbeli, P. Füglistaller, H. Zuber, *Biochim. Biophys. Acta* **1986**, *851,* 447.
[9] G. D. Scholes, *Annu. Rev. Phys. Chem.* **2003**, *54,* 57.
[10] C. Scharnagl, S. Schneider, *J. Photochem. Photobiol. B: Biol.* **1989**, *3,* 603.

[11] C. Scharnagl, S. Schneider, *J. Photochem. Photobiol. B: Biol.* **1991**, *8,* 129.
[12] Y. L. Ren, J. Wan, X. Xu, Q. Y. Zhang, G. F. Yang, *J. Phys. Chem. B* **2006**, *110,* 18665.
[13] J. Wan, X. Xu, Y. L. Ren, G. F. Yang, *J. Phys. Chem. B* **2005**, *109,* 11088.
[14] T. Förster, *Ann. Phys.* **1948**, *2,* 55.
[15] M. P. Debreczeny, K. Sauer, J. Zhou, D. A. Bryant, *J. Phys. Chem.* **1995**, *99,* 8412.
[16] M. P. Debreczeny, K. Sauer, J. Zhou, D. A. Bryant, *J. Phys. Chem.* **1995**, *99,* 8420.
[17] B. P. Krueger, G. D. Scholes, R. Jimenez, G. R. Fleming, *J. Phys. Chem. B* **1998**, *102,* 2284.
[18] G. D. Scholes, C. Curutchet, B. Mennucci, R. Cammi, J. Tomasi, *J. Phys. Chem. B* **2007**, *111,* 6978.
[19] C. Curutchet, G. D. Scholes, B. Mennucci, R. Cammi, *J. Phys. Chem. B* **2007**, *111,* 13253.
[20] A. Muñoz-Losa, C. Curutchet, I. F. Galván, B. Mennucci, *J. Chem. Phys.* **2008**, *129,* 034104.
[21] S. Speiser, *Chem. Rev.* **1996**, *96,* 1953.
[22] G. D. Scholes, R. D. Harcourt, *J. Chem. Phys.* **1996**, *104,* 5054.
[23] G. D. Scholes, R. D. Harcourt, K. P. Ghiggino, *J. Chem. Phys.* **1995**, *102,* 9574.
[24] R. D. Harcourt, G. D. Scholes, K. P. Ghiggino, *J. Chem. Phys.* **1994**, *101,* 10521.
[25] V. M. Agranovich, M. D. Galanin, Elementary energy transfer events, In Electronic Excitation Energy Transfer in Condensed Matter; V. M. Agranovich, A. Maradudin, Eds.; North-Holland: Amsterdam, **1982**,Chapter 1, p 8.
[26] T. Förster, In Modern Quantum Chemistry; O. Sinanoglu, Ed.; Academic Press: New York, **1965**;*III, pp.* 93–137.
[27] B. P. Krueger, G. D. Scholes, G. R. Fleming, *J. Phys. Chem. B* **1998**, *102,* 5378.
[28] M. E. Madjet, A. Abdurahman, T. Renger, *J. Phys. Chem. B* **2006**, *110,* 17268.
[29] D. Beljonne, J. Cornil, R. Silbey, P. Millie, J. L. Bredas, *J. Chem. Phys.* **2000**, *112,* 4749.
[30] K. F. Wong, B. Bagchi, P. J. Rossky, *J. Phys. Chem. A* **2004**, *108,* 5752.
[31] W. J. D. Beenken, T. Pullerits, *J. Chem. Phys.* **2004**, *120,* 2490.
[32] M. F. Iozzi, B. Mennucci, J. Tomasi, R. Cammi, *J. Chem. Phys.* **2004**, *120,* 7029.
[33] A. B. Doust, K. E. Wilk, P. M. G. Curmi, G. D. Scholes, *J. Photochem. Photobiol. A* **2006**, *184,* 1.
[34] C. D. van der Weij-De Wit, A. B. Doust, I. H. M. van Stokkum, J. P. Dekker, K. E. Wilk, P. M. G. Curmi, G. D. Scholes, R. van Grondelle, *J. Phys. Chem. B* **2006**, *110,* 25066.
[35] G. D. Scholes, G. R. Fleming, *J. Phys. Chem. B* **2000**, *104,* 1854.
[36] V. Sundstrm, T. Pullerits, R. van Grondelle. *J. Phys. Chem. B* **1999**, *103,* 2327.
[37] A. K. Padyana, V. B. Bhat, K. M. Madyastha, K. R. Rajashankar, S. Ramakumar, *Biochem. Biophys. Res. Commun.* **2001**, *282,* 893.
[38] A. D. Becke, *J. Chem. Phys.* **1993**, *98,* 5648.
[39] A. D. Becke, *Phys. Rev. A* **1988**, *38,* 3098.
[40] S. H. Vosko, L. Wilk, M. Nusair, *Can. J. Phys.* **1980**, *58,* 1200.
[41] R. Ditchfie, W. J. Hehre, J. A. Pople, *J. Chem. Phys.* **1971**, *54,* 724.
[42] S. Sinnecker, F. Neese, *J. Comput. Chem.* **2006**, *27,* 1463.
[43] M. R. A. Blomberg, P. E. M. Siegbahn, G. T. Babcock, *J. Am. Chem. Soc.* **1998**, *120,* 8812.
[44] O. A. Borg, B. Durbeej, *J. Phys. Chem. B* **2007**, *111,* 11554.
[45] V. I. Novoderezhkin, A. B. Doust, C. Curutchet, G. D. Scholes, R. van Grondelle, *Biophys. J.* **2010**, *99,* 344.
[46] M. J. Frisch, G. W. Trucks, H. B. Schlegel, G. E. Scuseria, M. A. Robb, J. R. Cheeseman, J. A. Montgomery, T. Vreven, K. N. Kudin, J. C. Burant, J. M. Millam, S. S. Iyengar, J. Tomasi, V. Barone, B. Mennucci, M. Cossi, G. Scalmani, N. Rega, G. A. Petersson, H. Nakatsuji, M. Hada, M. Ehara, K.; Toyota, R. Fukuda, J. Hasegawa, M. Ishida, T. Nakajima, Y. Honda, O. Kitao, H. Nakai, M. Klene, X. Li, J. E. Knox, H. P. Hratchian, J. B. Cross, V. Bakken, C. Adamo, J. Jaramillo, R. Gomperts, R. E. Stratmann, O. Yazyev, A. J. Austin, R. Cammi, C. Pomelli, J. W. Ochterski, P. Y. Ayala, K. Morokuma, G. A. Voth, P. Salvador, J. J. Dannenberg, V. G. Zakrzewski, S. Dapprich, A. D. Daniels, M. C. Strain, O. Farkas, D. K. Malick, A. D. Rabuck, K. Raghavachari, J. B. Foresman, J. V. Ortiz, Q. Cui, A. G. Baboul, S. Clifford, J. Cioslowski, B. B. Stefanov, G. Liu, A. Liashenko, P. Piskorz, I. Komaromi, R. L. Martin, D. J. Fox, T. Keith, A. Laham, C. Y. Peng, A. Nanayakkara, M. Challacombe, P. M. W. Gill, B. Johnson, W. Chen, M. W. Wong, C. Gonzalez, J. A. Pople, Gaussian 03; Revision D.01, Gaussian Inc: Wallingford, CT, **2004**.
[47] T. Gillbro, A. V. Sharkov, I. V. Kryukov, E. V. Khoroshilov, P. G. Kryukov, R. Fischer, H. Scheer, *Biochim. Biophys. Acta* **1993**, *1140,* 321.

Received: 17 July 2012
Revised: 5 December 2012
Accepted: 11 December 2012
Published online on 8 January 2013